AFRL-AFOSR-UK-TR-2024-0006

Multiscale Virtual Testing Capability for Composites (MUVITCAPCOM)

Carlos Gonzalez
FUNDACION IMDEA MATERIALES
CALLE DE ERIC KANDEL, 2
GETAFE, , 28906
ESP

12/11/2023
Final Technical Report

Air Force Research Laboratory
Air Force Office of Scientific Research
European Office of Aerospace Research and Development
Unit 4515 Box 14, APO AE 09421

REPORT DOCUMENTATION PAGE

PLEASE DO NOT RETURN YOUR FORM TO THE ABOVE ORGANIZATION.

1. REPORT DATE	2. REPORT TYPE	3. DATES COVERED	
20231211	Final	START DATE 20190901	END DATE 20230831

4. TITLE AND SUBTITLE
Multiscale Virtual Testing Capability for Composites (MUVITCAPCOM)

5a. CONTRACT NUMBER	5b. GRANT NUMBER	5c. PROGRAM ELEMENT NUMBER
	FA9550-19-1-7036	
5d. PROJECT NUMBER	**5e. TASK NUMBER**	**5f. WORK UNIT NUMBER**

6. AUTHOR(S)
Carlos Gonzalez

7. PERFORMING ORGANIZATION NAME(S) AND ADDRESS(ES)
FUNDACION IMDEA MATERIALES
CALLE DE ERIC KANDEL, 2
GETAFE 28906
ESP

8. PERFORMING ORGANIZATION REPORT NUMBER

9. SPONSORING/MONITORING AGENCY NAME(S) AND ADDRESS(ES)	10. SPONSOR/MONITOR'S ACRONYM(S)	11. SPONSOR/MONITOR'S REPORT NUMBER(S)
EOARD UNIT 4515 APO AE 09421-4515	AFRL/AFOSR IOE	AFRL-AFOSR-UK-TR-2024-0006

12. DISTRIBUTION/AVAILABILITY STATEMENT
A Distribution Unlimited: PB Public Release

13. SUPPLEMENTARY NOTES

14. ABSTRACT
The MUVITCAPCOM (Multiscale Virtual Testing Capability for Composites) project focuses on advancing the understanding of composite materials through multiscale modelling, specifically targeting fibre-reinforced carbon epoxy composites by collaborative research between AFRL and IMDEA Materials Institute. The research incorporates advanced micromechanical testing techniques to analyze the material's behaviour at various scales, including fibre push-in, matrix pillar compression and cantilever beams machined with focus FIB. By integrating experimental data from micromechanical tests with computational models, the project aims to enhance the predictive accuracy of simulations at both micro and macro scales. This approach enables a comprehensive investigation into the complex interactions between individual fibres and the epoxy matrix, offering insights into the material's overall mechanical properties. The goal is to optimize the design and performance of composite materials for diverse applications, such as aerospace industries, by providing a more accurate and reliable framework for understanding and predicting their behaviour under different conditions

15. SUBJECT TERMS

16. SECURITY CLASSIFICATION OF:			17. LIMITATION OF ABSTRACT	18. NUMBER OF PAGES
a. REPORT	b. ABSTRACT	c. THIS PAGE		
U	U	U	SAR	18

19a. NAME OF RESPONSIBLE PERSON	19b. PHONE NUMBER *(Include area code)*
DAVID SWANSON	785-6565

Standard Form 298 (Rev.5/2020)
Prescribed by ANSI Std. Z39.18

MUVITCAPCOM

Multiscale Virtual Testing Capability for Composites

AWARD NO: FA9550-19-1-7036

PRINCIPAL INVESTIGATOR: Carlos González

Period of performance: 9/1/2019-8/31/2023

FINAL PERFORMANCE REPORT

(9/1/2019-8/31/2023)

"This material is based upon work supported by the Air Force Office of Scientific Research under award number FA9550-19-1-7036."

"Any opinions, findings, and conclusions or recommendations expressed in this material are those of the author(s) and do not necessarily reflect the views of the United States Air Force."

MUVITCAPCOM project:

- Federal Agency and Organizational Element to Which Report is Submitted: AFOSR (Air Force Office of Scientific Research)
- Federal Grant or Other Identifying Number Assigned by Federal Agency: Fundación IMDEA Materiales (IMDEA)
- DUNS Number: 4600334930000
- EIN: G84908953

For more information on this document or MUVITCAPCOM, please contact:

Dr. Carlos González
carlosdaniel.gonzalez@imdea.org
Fundación IMDEA Materiales
Eric Kandel, 2
Parque Científico y Tecnológico - Tecnogetafe
28906 Getafe (Madrid) SPAIN
Tel: +34 91 549 3422
http://www.materials.imdea.org/

Dr. Davide Mocerino
davide.mocerino@imdea.org
Fundación IMDEA Materiales
Eric Kandel, 2
Parque Científico y Tecnológico - Tecnogetafe
28906 Getafe (Madrid) SPAIN
Tel: +34 91 549 3422
http://www.materials.imdea.org/

TABLE OF CONTENTS

1 LIST OF FIGURES

2 SUMMARY

Multiscale simulation strategy for composites can drive more efficient and safer structural parts in airplanes and cars. Because of the complex damage behavior of composites materials, the numerical models must be validated against experimental data. To improve the numerical and experimental approaches of the fracture mechanics in composites, the teams at AFRL and IMDEA MATERIALS have started to walk together sharing their knowledge and experience in the field. The experimental methodologies developed to study the interface between fiber and matrix developed during the second year of the project was completed and deeply analyzed performing a great number of experiments, assisted by the numerical part to confirm and help top obtaining the right behavior of the interface. The research lines that the task of the project have brought to light, despite COVID-19 situation were analyzed carefully and the obtained results are reported with all the benefits for the understanding of the fractures mechanism and the interface properties at micro-level. This last extension report contains the main results obtained in a new experimental campaign devoted to characterizing the interface strength and toughness of UD structural composites.

3 INTRODUCTION

In contemporary engineering, fiber-reinforced composite materials with polymer matrices find widespread use in structural components for airplanes and cars. However, the certification of these structural parts often involves overestimated safety factors due to the intricate fracture behavior exhibited by these composite materials. Addressing the economic challenges associated with design and certification, there is a need for advanced fracture mechanical models [1,2]. These models not only enhance the understanding of damage behavior but also provide a cost-effective alternative to expensive experimental tests by utilizing virtual simulations for certification purposes.

Various approaches exist for modeling the fracture mechanics of composites, each with its advantages and disadvantages. Notably, research teams at AFRL and IMDEA MATERIALS employ distinct fracture models and methodologies [3,4]. The primary objective of the project is to foster collaboration and knowledge exchange in both experimental and computational micromechanics. The aim is to enhance both approaches by integrating their best features. To facilitate this collaboration, six work packages have been defined, each corresponding to specific collaboration topics. Table 1 outlines the work packages and their respective tasks.

Table 1. Work packages of the project with their tasks.

Work package	Tasks
WP1 - Characterization of missing properties	Model of single-fiber cruciform test (CDM) X-ray and synchrotron imaging single-fiber cruciform test New setup single-fiber test, carbon fiber
WP2 - Increasing realism in microstructural modelling	Implementation of long term microstructural features in RVE, fiber clustering MicroRVE simulations with long term microstructural features Statistical information from digitized micrographs Validation of microRVE with microDIC (SEM)
WP3 - Cross-validation and cross-enhancement of damage propagation approaches	Simulation crack propagation through ply using RX-FEM Transfer model geometries between AFRL and IMDEA Transfer model inputs between CDM-IMDEA and DDM-AFRL Micro-meso homogenization crack propagation (cohesive law)
WP4 - Development of experimental procedures for crack propagation assessment	Experimental setup 3-point-bending test Experimental setup Brazilian test Model of 3-point-bending test, embedded microstructure Model of Brazilian test, embedded microstructure Experimental setup ENF test
WP5 - Microstructural quantification	Nano-XCT scan of micro machined pillars Preparation of micro machined pillars Post-process of micro XCT scans from pillars
WP6 - Validation of the computational approaches	Setup and experimental compression of micro machined pillars Model of micro machined pillar

Over the past year, the work conducted within WP6 has delved deeper into achieving a harmonious balance between the fracture process of the pillar and the plastic behavior of the matrix. Various case studies involving different materials parameters are presented to demonstrate the modifications made to achieve optimal alignment between experiments and models.

The micromechanical tests undertaken in recent years to obtain missing properties in the microlevel characterization of a composite (WP1) focused on the application of cantilever tests to deduce interface properties between fibers and the matrix. The optimization of micro-cantilever tests involved the utilization of the Focus Ion Beam to fabricate specimens subsequently subjected to testing.

This experimental work was complemented by simulations, aiming to fine-tune both material and interface models to ensure a robust alignment with the experimental curves.

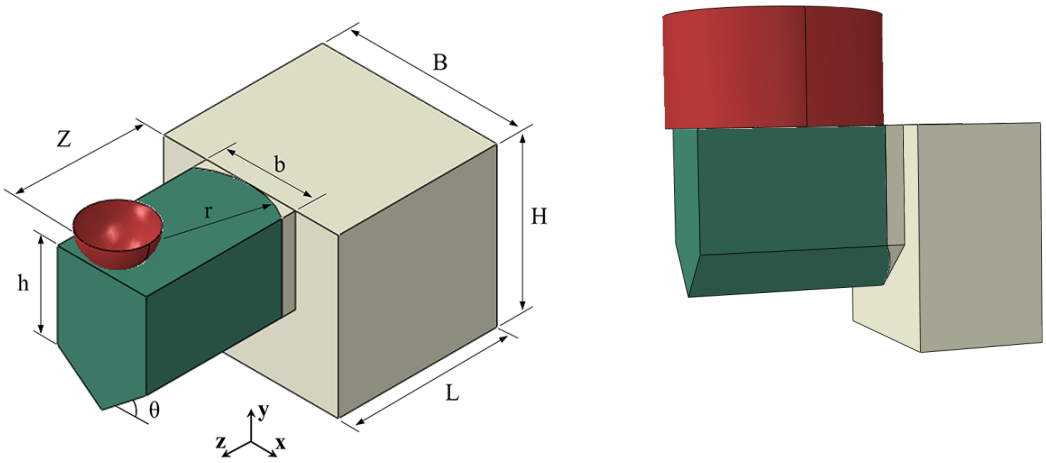

Figure 1. Geometrical schematization of microcantilever MODE I and MODE II

The last step was the generalization of the developed model, trying to extrapolate an analytical law able to predict the fracture energy without the use of the FEM models, but only using some experiments to be sure of the geometrical dimension of the specimens.

Finally, it is noteworthy that regular meetings between IMDEA MATERIALS and AFRL were useful in order to share experimental and numerical results.

4 METHODS, ASSUMPTIONS AND PROCEDURES

Over the past year, two key initiatives were pursued:

1. **Micro-Pillar Experiment Finite Element Models:**
    - *Methods*: Developed detailed finite element models replicating fracture and deformation in micro-pillar experiments.
    - *Results*: Successfully mimicked experimental fracture patterns and validated against actual data.
2. **Cantilever for Micro-Mechanical Characterization:**
    - *Methods:* Created a numerical model for a cantilever, focusing on micro-mechanical characterization of interface strength and fracture energy.
    - *Results*: Provided insights into interface strength, quantified fracture energy, and conducted sensitivity analyses.

In summary, these efforts enhance our understanding of material behavior at the micro-scale, achieved through advanced simulations and focused mechanical characterization.

Reproduction with Finite Element Model of deformation and Fracture evolution of Micropillar

IMDEA MATERIALS developed a comprehensive numerical model in Abaqus software to replicate the micro-pillar compression tests conducted by AFRL. The model encompasses the full experimental setup and utilizes data extracted from SEM microscope experiments to define its geometry. To accurately capture the experimental conditions, variations in fiber radius and the positioning of fibers were incorporated, ensuring alignment with the experimental setup, as illustrated in Figure 2. The design of the model considered the inherent variability in the radius of fibers and their placement, closely mirroring the experimental conditions.

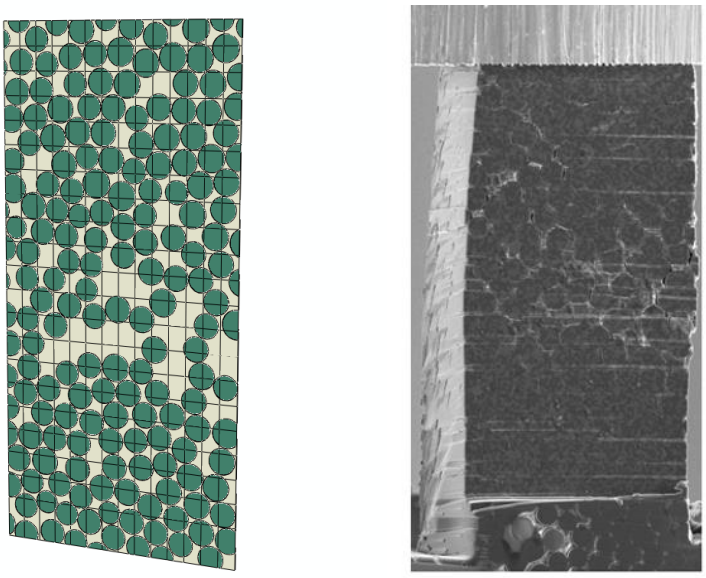

Figure 2. Developed Model of Micropillar

As previously specified, the fibers exhibit transversely isotropic elastic behavior, while the matrix is characterized by an isotropic elastoplastic model coupled with continuum damage behavior, incorporating plasticity in both compressive and tensile loading scenarios [5].

For the fiber-matrix interface, a cohesive law was employed, specifically a linear traction-separation law utilizing the Benzeggagh-Kenane mixed-mode model. A quadratic failure initiation criterion was applied.

Analytical formulation based on carbon fiber cantilever

We investigated the properties between the matrix and fibers through the utilization of micro-cantilevers. This innovative approach allows for the determination of interface properties in fiber-reinforced materials. The microcantilever geometry was designed based on 3D finite element simulations, and subsequently, physical specimens were created using the Focus Ion Beam (FIB) device at IMDEA MATERIALES.

The finite element model represents a micro-cantilever with dimensions matching those of the specimens produced with the FIB. The matrix and fiber are treated as independent parts, connected through cohesive behavior featuring a linear traction-separation law, incorporating the Benzeggagh-Kenane model and a quadratic failure initiation criterion.

Employing a systematic methodology with the FIB, regular micro-cantilevers were fabricated, each with a length of 5 microns, a height of 3 microns, and a width of 3 microns. Subsequently, these micro-cantilevers underwent testing using a nano-indenter machine (Hystron).

Moreover, as mentioned earlier, having an analytical formulation proves particularly beneficial as it enables a direct determination of interface properties from experimental results, bypassing the lengthy and time-intensive numerical simulations. This methodology was employed to estimate both interface strength and fracture energy, validated against experimental evidence.

The analytical approach involved a microcantilever beam elastic scheme, depicting shear force and bending moment distributions as illustrated in Figure 3 (a). The shear stress (τ) and bending moment stress (σ) depend on the elastic and geometrical properties of the beam, such as cantilever length, section moment of inertia, and material elastic modulus. This is further illustrated in Figure 3 (b), presenting a sectional side view of the micro-beam. Within certain limits of beam geometry and deflection, the Euler-Bernoulli and Timoshenko theories provide a comprehensive analytical description of the elastic problem before the initiation of interface debonding.

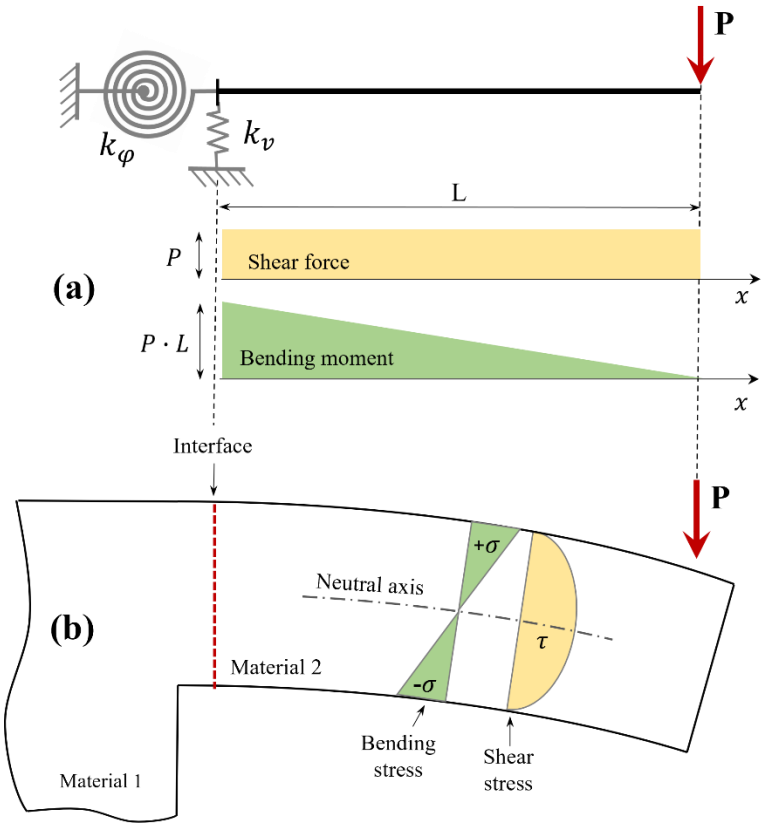

Figure 3: Micro-cantilever beam elastic scheme with elastic constraints (a) and a section side view of the micro beam with stress distribution and interface positioning (b)

The kinematic relation establishes a connection between strain fields and displacement, as well as rotation through a differential approach. Simultaneously, the equilibrium differential equations, tailored for the specific load configuration under consideration, succinctly express the correlation between bending moment and shear load. Furthermore, these equations capture the continuity of shear load along the length of the beam.

$$M_z(x) = P_y \cdot x = E_x I_z \frac{d\varphi_z(x)}{dx} \quad (1)$$

$$P_y(x) = k_s A G_{xy} \left(\varphi_z - \frac{du_y(x)}{dx}\right) \quad (2)$$

The solution devised for the beam needs adaptation when there's an interface surface within the specimen. This surface, often representing a discontinuity, serves to connect two distinct materials.

5 RESULTS AND DISCUSSION

The main results of the developed tasks are discussed in this section.

Reproduction with Finite Element Model of deformation and Fracture evolution of Micropillar

The initial material parameters for fibers, matrix, and the interface were derived from a blend of information found in the literature and insights gained from prior simulations of carbon fiber-epoxy systems. Following this, a case-sensitive study was conducted to fine-tune these parameters. The outcomes of the sensitivity study on the materials parameters are depicted in Figure 4.

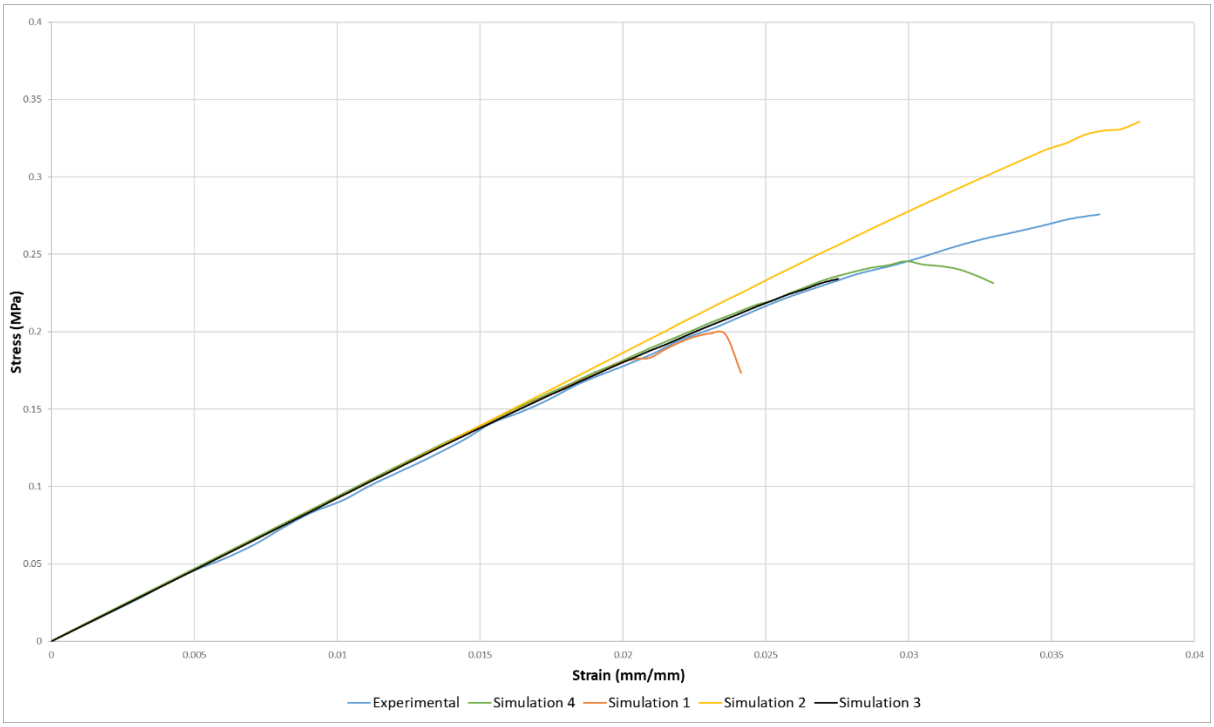

Figure 4: Sensitivity study of Interface Material parameters for Micropillar tests

Case/Parameter	σ [GPa]	T_{12}[GPa]	T_{23}[GPa]	G_I [nJ/µm²]	G_{II} [nJ/µm²]	G_{III} [nJ/µm²]
Simulation 1	0.032	0.05184	0.05184	0.12	0.12	0.12
Simulation 2	0.1	0.135	0.135	0.01	0.1	0.1
Simulation 3	0.032	0.05184	0.05184	0.01	0.1	0.1

After achieving a close alignment between the results of Simulation 3 and experimental data, adjustments were implemented to the matrix plasticity model and damage for Simulation 4. The evolution curve detailing plasticity and damage in the matrix throughout this simulation is presented below.

Parameters	Yeld Stress [GPa]	Inelastic Strain
Concrete Compression Hardening	0.186 0.187 0.002	0 0.32 0.45
Concrete Tension Stiffening	0.137 0.138 0.002	0 0.32 0.55
Concrete Compression Damage	0 0 0.1	0 0.32 0.45
Concrete Tension Damage	0 0 0.1	0 0.32 0.45

Concerning boundary conditions, the configuration reproduced constraints on the lower section of the micro-pillar geometry. Additionally, a velocity in the compression direction was applied to the upper surface. The simulations presumed plane strain conditions in the direction of the fibers and embraced a quasi-static response.

Micro-mechanical analytical solution based on experimental tests.

To incorporate the classical Timoshenko model for the beam in the presence of an interface, it becomes imperative to account for constraint conditions that deviate from the ideal full fixity. The schematic representation of these conditions proves to be particularly intricate. Given that the microcantilever specimen is created by milling the beam within a continuous material block, the overall compliance of the specimen is influenced by the material surrounding the beam. Hence, it is deemed to be elastically constrained, and the compliance of the different material blocks (k_φ and k_v) should be taken into consideration.

By integrating the preceding equation (1 and 2) and isolating terms, the final form, considering compliance, is derived.

$$\varphi_z(x) = \frac{x \cdot P_y}{E_x I_z}\left(\frac{x}{2} - L\right) + \frac{P_y L}{k_\varphi}$$

$$u_y(x) = \frac{x \cdot P_y}{k_s A G_{xy}} + \frac{x^3 \cdot P_y}{2E_x I_z}\left(L - \frac{x}{3}\right) + \frac{P_y}{k_v}$$

The proposed procedures, while still incorporating numerical methods, prove to be significantly more efficient in terms of both time and computational costs when compared to the cohesive modelling approach. The required simulations involve establishing the relationship between the entire specimen's compliance and the advancement of the debonding front. Collectively, these simulations take only a fraction of the time required for a single simulation with the cohesive model implemented.

To ensure the consistency of the Timoshenko theory with respect to the considered problem, a comparison between numerical and analytical beam deflection curves was conducted. For this purpose, the fiber beam was modelled numerically as an independent entity, rigidly constrained at one end and vertically loaded at the other end. Subsequently, the bending stress distribution was assessed over a beam section located far from both the constrained and loaded sections. Figure 5 illustrates the schematization of the deflection line identification procedure, which is compared to a contour plot of U2 displacements over the fiber beam.

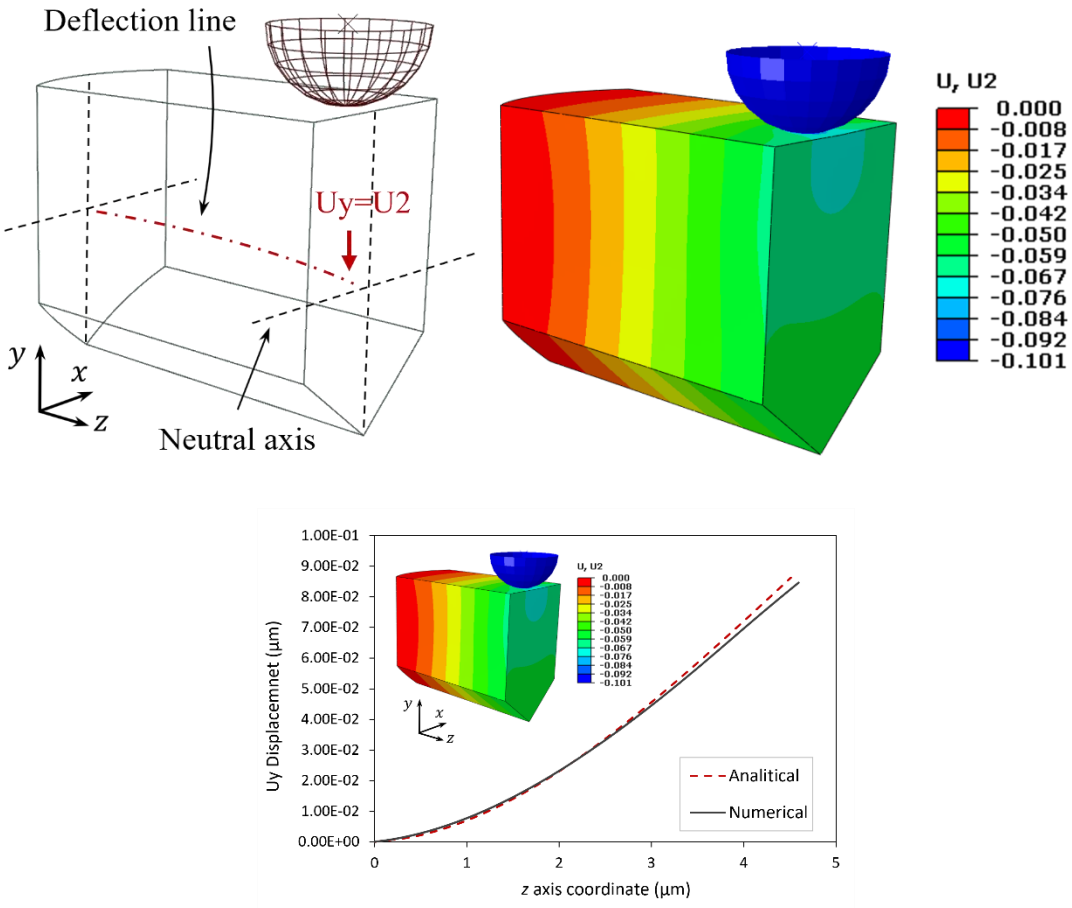

Figure 5. Schematization of the numerical deflection line identification procedure on the left and U2[µm] displacements contour plot on the right and respectively comparison between analytical and numerical solution.

Displacements along the beam axis were analytically computed based on known fiber properties and beam geometry. The section moment of inertia and neutral axis position were calculated under the assumption of pure bending loading conditions. Both the numerical model and the analytical procedure were calibrated, with respect to geometry, using data from experimental tests.

To analytically define the micro-cantilever specimen's deflection curve under the testing conditions, considering the effect of matrix compliance, elastic constraint stiffnesses (k_φ and k_v) were calibrated on the elastic response of the matrix block. A numerical simulation involving the entire micro-cantilever specimen measured the displacement Uy of the interface section centre of gravity and the average rotation of that section. With the applied load and geometrical

dimensions known, compliances could be estimated. The results give a good agreement between numerical approach and the use of Timoshenko formulation.

As the contact surface is not flat, the displacement field on its intersection with the deformation axis surface is not constant. Figure 6 presents contour plots representing displacements along the y-axis and axial z-displacements, showing minimal changes in U_y over the interface front and an almost perfectly linear distribution of axial U_z displacements along the section height. As in Figure 5 the analytical approach is well matching the FEM results.

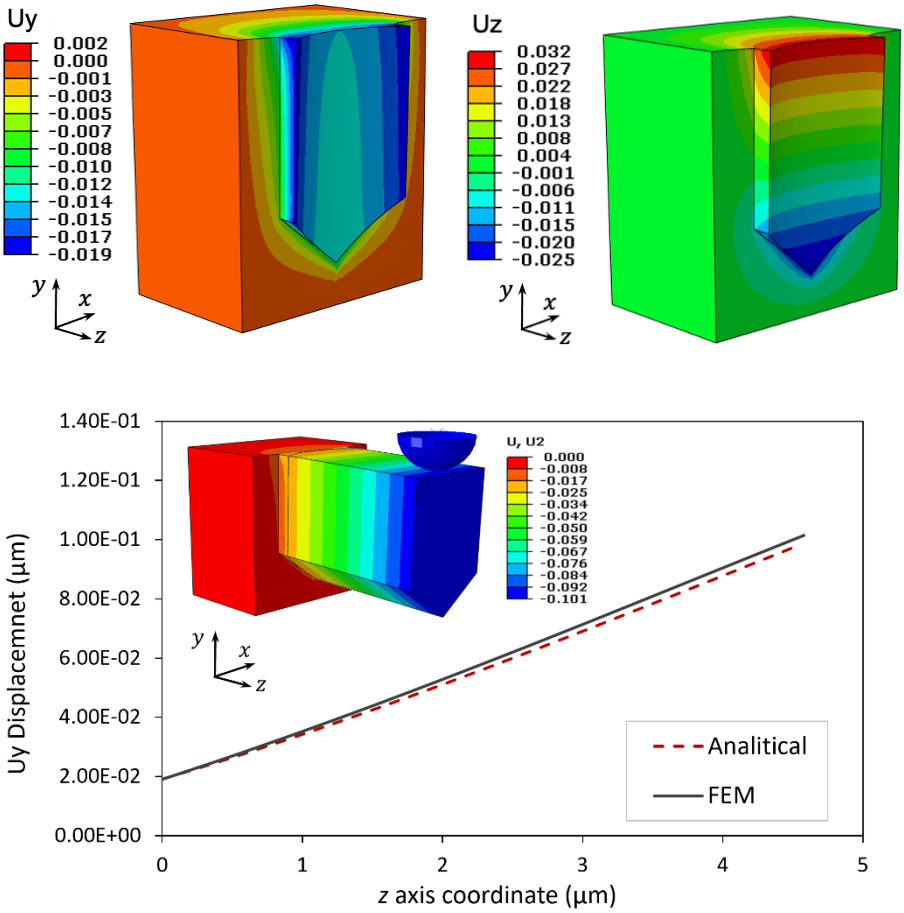

Figure 6. Interface section displacement fields U_y and U_z reported in [µm], and comparison of FEM solution with the analytical model.

After confirming that the deformation regime of the specimens is equivalent to that of a bending beam, a regression to determine the interface strength properties can be conducted. With the known geometrical and inertial properties of the beam cross-section, the bending stress at the upper surface of the section can be calculated using the continuum mechanics equation.

$$\sigma = \frac{M_z}{I_z} \cdot y_{max} = \frac{P \cdot L}{I_z} \cdot y_{max}$$

where all the properties are well defined, and P is extrapolated from the experimental load vs depth curves.

In conclusion, the determination of interface strength involved analysing the average load over the depth curve for the mode I test experiments. Figure 7 displays its value over depth alongside the average load P. Notably, the load derivative remains quasi-constant for an initial depth amplitude, followed by a rapid drop. The average value within the initial constant range was computed. The depth corresponding to the first drop in the derivative value was then used to define the load value P=153.4 µN, corresponding to the debonding onset and resulting in σ=102.64 MPa.

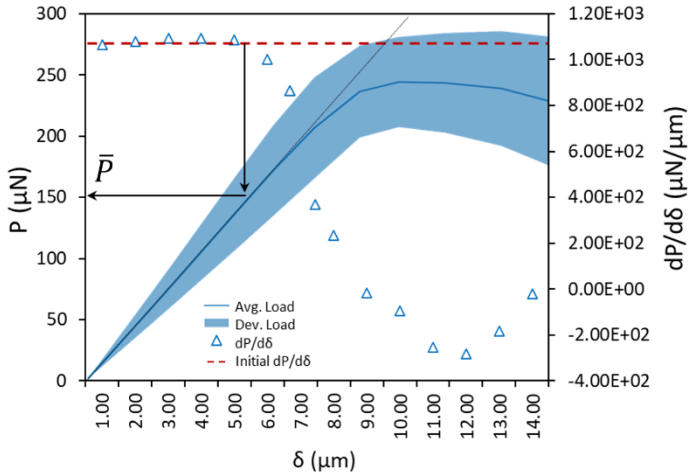

Figure 7. Average load vs depth curve for the mode I tested specimens, together with its discrete derivative and the mean value of the initial range where this last is constant

An analytical procedure for deducing interface properties from experimental results was also proposed for toughness identification. The tests involved a cyclic process of partial unloading during their execution, as illustrated in Figure 8. Each loading ramp exhibited a load vs. depth slope, representing the specimen stiffness at that particular stage. Notably, the slopes displayed two distinct phases. In the initial phase, they remained quasi-constant across loading steps, while in the subsequent phase, a gradual reduction in slopes was observed.

In the absence of other dissipation phenomena (such as plastic deformation, indenter tip sliding, indentation, etc.), the progressive decrease in specimen stiffness is attributed to the onset and propagation of debonding. Therefore, retracing the decrease in loading slopes proves valuable in identifying the stage of debonding progression. This approach, grounded in Griffith's energetic principles, is a widely adopted practice for estimating toughness in both fracture and adhesive joint mechanics. It enables the computation of the energy release rate based on the testing load conditions, geometrical configuration, and crack advancement. Two generic subsequent load cycles present stiffnesses respectively equal to K_{i-1} and K_i and corresponding debonding length a_{i-1} and a_i.

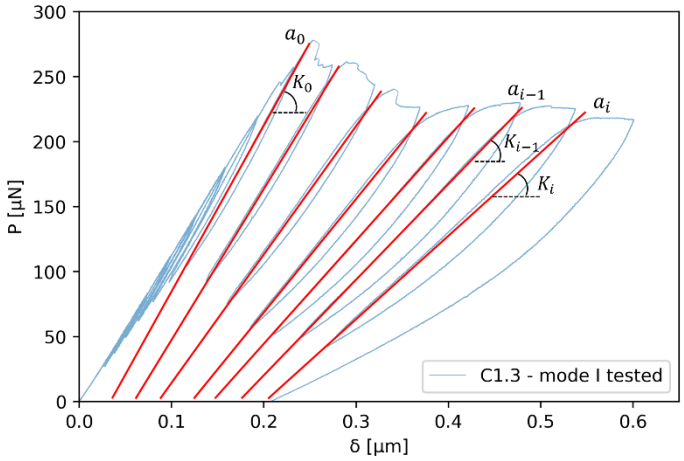

Figure 8. Schematization of the experimental stiffness identification with the debonding cycling progression.

The Griffith energy balance was used to obtain a discrete form of the equation for energy calculation.

$$G_i = \frac{P_i^2}{2B} \cdot \frac{C_i - C_{i-1}}{a_i - a_{i-1}}$$

The calculated value of toughness was compared to that numerically obtained showing the robustness of used calculation methodologies.

The resulting specimen compliance-debonded length pairs were interpolated with a polynomial function.

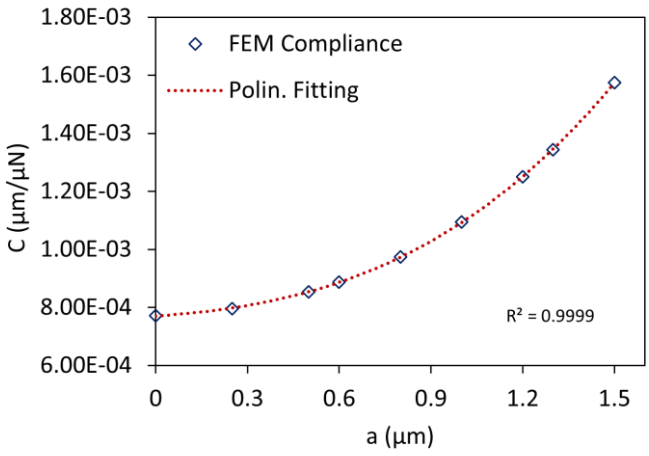

Figure 9. Numerically calculated compliance vs debonding length data and cubic polynomial fitting curve, together with the R-squared value.

The best fitting resulted from the adoption of a third-order complete polynomial, here reported in general form:

$$C(a) = A_1 \cdot a^3 + A_2 \cdot a^2 + A_3 \cdot a + C(a = 0)$$

Where C(a=0) it is a compliance for a completely bonded interface, thus it should not be calculated by the fitting process.

The equation allows to estimate the debonding length increment Δa for each of the compliance intervals experimentally defined. On the basis of these presented data the energy release rate was calculated and reported in Figure 10.

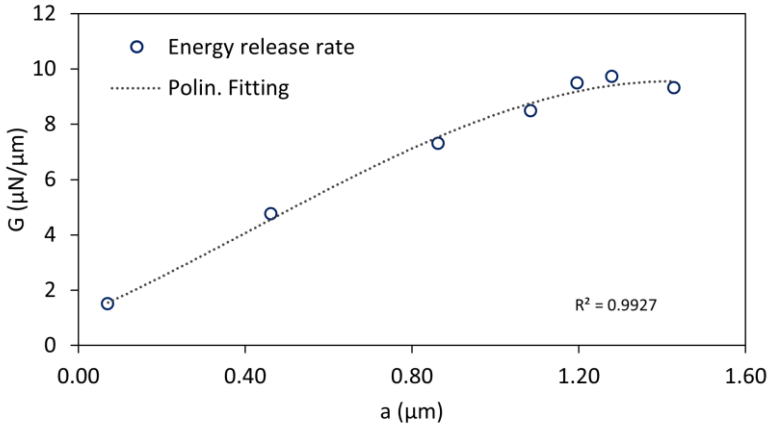

Figure 10. Energy release rate G over debonding length a

Observing the initial phase of debonding propagation, it becomes evident that the energy release rate G linearly increases with the advancement of debonding, denoted as 'a'. In the later phase of damage propagation, the values of G converge toward a finite value. This upper limit for the energy release rate is close to 10 µN/µm. Given that the load cycles corresponding to this limit value demonstrate the most stable propagation in terms of load vs. depth curve, this identified limit value was adopted as the interface toughness.

6 CONCLUSIONS

The finite element models developed during this year gave good results about the fracture mechanism of a Micropillar coupon, meanwhile, the interface strength of the fibre-reinforced composite is well represented by analytical considerations.

The main technical conclusions from the current results are summarized in the following list.

- Caution is required in managing the matrix damage model at the microscale. While it is necessary for the matrix damage to exhibit brittleness at this scale, it is equally important to permit a degree of plastic behavior prior to reaching this brittle failure.
- It's crucial to approach the matrix damage model at the microscale thoughtfully. While the desired behavior is brittleness at this level, it's equally important to incorporate a certain level of plasticity before reaching the point of brittle failure.
- The analytical formulation of carbon fiber micro-cantilevers enables the direct calculation of interface material properties, resulting in significant savings in computational time and costs.

7 REFERENCES LIST OF SYMBOLS, ABBREVIATIONS AND ACRONYMS

[1] European Union Aviation Safety Agency. Certification Specifications and Acceptable Means of Compliance for Large Aeroplanes CS-25, Amendment 23 2019.
[2] Ostergaard MG, Ibbotson AR, Roux OL, Prior AM. Virtual testing of aircraft structures. CEAS Aeronaut J 2011;1:83–103. https://doi.org/10.1007/s13272-011-0004-x.
[3] Lopes CS, González C, Falcó O, Naya F, LLorca J, Tijs B. Multiscale virtual testing: the roadmap to efficient design of composites for damage resistance and tolerance. CEAS Aeronaut J 2016;7:607–19. https://doi.org/10.1007/s13272-016-0210-7.
[4] Iarve EV, Gurvich MR, Mollenhauer DH, Rose CA, Dávila CG. Mesh-independent matrix cracking and delamination modeling in laminated composites. Int J Numer Methods Eng 2011;88:749–73. https://doi.org/10.1002/nme.3195.
[5] Fiedler B, Hojo M, Ochiai S, Schulte K, Ando M. Failure behavior of an epoxy matrix under different kinds of static loading. Compos Sci Technol 2001;61:1615–24. https://doi.org/10.1016/S0266-3538(01)00057-4.